Microscopic Superfluidity in ^{4}He Clusters Stirred by a Rotating Impurity Molecule

Angeline Wairegi,[1] Antonio Gamboa,[2] Andrew D. Burbanks,[3] Ernestine A. Lee,[4] and David Farrelly[1,*]
[1]Department of Chemistry and Biochemistry, Utah State University, Logan, Utah 84322-0300, USA
[2]Institut de Sciences Moléculaires d'Orsay, CNRS UMR 8214, Université de Paris-Sud 11, Bâtiment 210, F91405, Orsay Cedex, France
[3]Department of Mathematics, University of Portsmouth, Portsmouth, P01 3HF, United Kingdom
[4]FivePrime Therapeutics, Two Corporate Drive, South San Francisco, California 94080, USA
(Received 25 November 2013; published 11 April 2014)

The effective moment of inertia of a CO impurity molecule in ^4He_N and p-$(H_2)_N$ solvent clusters initially increases with N but then commences a nonclassical decrease at $N = 4$ (^{4}He) or $N = 6$ (p-H_2). This suggests molecule-solvent decoupling and a transition to microscopic superfluidity. However, the quantum decoupling mechanism has not been elucidated. To understand the decoupling mechanism, a one-dimensional model is introduced in which the ^{4}He atoms are confined to a ring. This model captures the physics and shows that decoupling happens primarily because of bosonic solvent-solvent repulsion. Quantum Monte Carlo and basis set calculations suggest that the system can be modeled as a stirred Tonks-Girardeau gas. This allows the N-particle time-dependent Schrödinger equation to be solved directly. Computations of the integrated particle current reveal a threshold for stirring and current generation, indicative of superfluidity.

DOI: 10.1103/PhysRevLett.112.143401 PACS numbers: 36.40.−c, 02.70.Ss, 67.25.dw

Impurity molecules doped into small bosonic clusters consisting of ^{4}He or p-H_2 solvent particles appear to decouple from their environment as the cluster grows in size [1–6]. Decoupling is suggested experimentally by sharp, free-molecule-like, rotational lines in the spectra and has been attributed to the onset of a new phenomenon —microscopic superfluidity [5–10]. However, the relationship between microscopic superfluidity and conventional (bulk) superfluidity remains largely unexplored. The onset of microscopic superfluidity is inferred from the nonclassical turnaround and subsequent increase in the effective rotational constant ($B_{\rm eff}$) of the molecule (a decrease in the effective moment of inertia) as the number (N) of solvent particles is increased [4,7,10,11]. Microscopic (or mesoscopic) superfluidity also occurs in cold-atom physics and, in particular, low-dimensional ultracold gases [12–14]. For example, theoretical studies demonstrate that a one-dimensional (1D) gas of impenetrable bosons—a Tonks-Girardeau (TG) gas [15–17]—constrained to a ring of finite circumference displays a critical velocity below which the system is hard to stir. If the stirring perturbation is a δ-function barrier then it experiences a zero drag force except at certain stirring velocities [18]. Here we demonstrate that the physics of microscopic superfluidity in bosonic solvents shares much in common with a stirred TG gas with the barrier replaced by a rotating impurity molecule. This finding allows the N-body time-dependent Schrödinger equation (TDSE) to be solved numerically. In particular, computations of the integrated particle current uncover key signatures of superfluidity [12].

The decoupling of impurity molecules from the bosonic solvent has previously been attributed to superfluidity in path integral Monte Carlo (PIMC) simulations [10]. Using the two-fluid model, in p-$(H_2)_N$-CO clusters, both a normal and a superfluid component were found to coexist. The main finding of the PIMC calculations was a superfluid fraction that declined from about 95% at $N = 1$ to about 82% at $N = 6$, followed by an increase to essentially 100% for $N > 10$. These calculations provide excellent agreement with the experimentally observed behavior of $B_{\rm eff}$ for $N < 10$, as do previous 0 K quantum Monte Carlo simulations [19–21]. Nevertheless, as emphasized in a recent review [6], while PIMC can simulate essentially all properties of superfluid ^{4}He, it does so by projecting the system onto a classical analogy. This may make it difficult to draw direct conclusions about the actual quantum behavior. For example, the reporting of a normal and a superfluid fraction for $N = 1$ [10] is difficult to interpret physically. Furthermore, there no unique definition of microscopic superfluidity [12], and the quantum decoupling mechanism itself has not previously been elucidated.

Our objective is to understand how the decoupling mechanism occurs and also whether calculations of the particle current density indicate superfluid behavior. The latter calculation requires the solution of the $(N + 1)$-body TDSE, which is clearly not possible for the full-dimensionality problem. Therefore, we construct a reduced-dimensionality model of the ^4He_N-CO system with the ^{4}He atoms confined to a ring as shown in Fig. 1 (not to be confused with Lehmann's very useful but nevertheless "toy" model [22]). This model has the felicitous property that it permits accurate quantum basis set computations for $N \leq 5$. Using quantum Monte Carlo calculations, we first demonstrate that the model contains the essential physics,

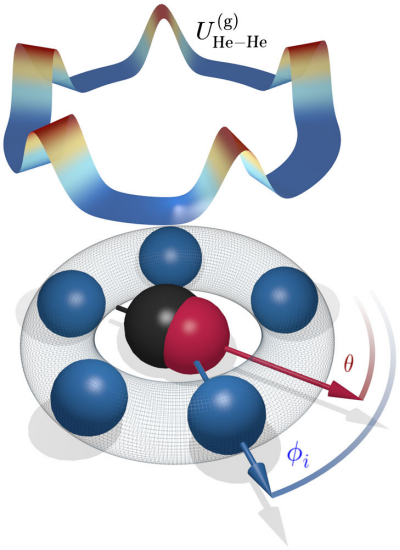

FIG. 1 (color online). Bosons-on-a-ring (BOAR) model. The ^{4}He atoms (blue) are confined to revolve on a ring of radius R_0 measured from the center of mass of the CO molecule (black/red). The molecule is pinned at the origin and rotates in the plane of the ring. The azimuthal angles of the molecule and the ith ^{4}He atom are θ and ϕ_i, respectively. The ribbon above the ring illustrates the soft Gaussian repulsive potential, $U^{(g)}_{He-He}$, as a function of the angles between the He atoms.

that is, the turnaround in B_{eff}. The calculations suggest a further simplification: modeling the problem as a stirred TG gas. It is this step that allows us to solve the TDSE directly for N ^{4}He atoms stirred by the molecule.

The Hamiltonian, in the limit of the BOAR approximation (see Fig. 1), is

$$\hat{H} = \frac{\hat{j}_z^{\,2}}{2I_{CO}} + \sum_{i=1}^{N}\left[\frac{\hat{\ell}_{iz}^{\,2}}{2mR_0^2} + V(\phi_i - \theta)\right] + \sum_{i<k}^{N} U(\phi_i - \phi_k), \tag{1}$$

where I_{CO} is the moment of inertia of the CO molecule and $\hat{j}_z$ is the molecular rotational angular momentum (AM) operator; the quantity $\hbar^2/2mR_0^2 \sim 0.19$ cm^{-1} is used to define a moment of inertia $I_0 = mR_0^2$; $\hat{\ell}_{iz}$ is the orbital AM operator for the ith ^{4}He atom (mass m), and ϕ_i and θ are the angles shown in Fig. 1. The atom-molecule potential energy surface (PES) is $V(\phi_i - \theta)$, and the PES of Ref. [23] is used. The He-He PES is $U(\phi_i - \phi_k)$. Based on previous diffusion Monte Carlo calculations [19], we set $R_0 = 9$ bohr throughout. The gas phase rotational constant for CO is $B_0 = 1.9225125$ cm^{-1} [4]. Two reference angular frequencies are introduced for future use: $\omega_0 = \hbar/I_0$ and $\omega_{eff} = \hbar/I^{eff}_{CO}$, where I^{eff}_{CO} is an effective moment of inertia that will be varied.

To further simplify the Hamiltonian, the ^{4}He-CO PES is expanded in Legendre polynomials with only the first three (dominant) terms being retained, i.e., $V(R,\Theta) = \sum_{n=0}^{n=2} V_n(R_0)P_n(\cos\Theta)$ where $\Theta = \phi_i - \theta$. Actually, in the BOAR model, the isotropic V_0 contribution is simply an additive constant. Three forms for the He-He PES are used: (i) the empirical PES of Aziz, McCourt, and Wong (AMcW) [24], (ii) a purely repulsive Gaussian barrier, and (iii) a δ-function potential as in the TG gas. The Gaussian barrier is given by $U^{(g)}_{He\text{-}He}(\phi_{ij}) = g_0 e^{-\alpha\phi_{ij}^2}$, where ϕ_{ij} is the angle between the ith and jth ^{4}He atom (see Fig. 1). The Gaussian approximation interpolates between the actual AMcW PES and the TG limit. In addition, its functional form simplifies the calculation of matrix elements as compared to the AMcW PES. Two sets of parameters for the Gaussian barrier are used (see the caption to Fig. 2) corresponding to a hard and a soft barrier. The soft Gaussian, shown as the ribbon in Fig. 1, roughly models the actual van der Waals radius of the ^{4}He atoms, whereas the much harder barrier lies closer to the TG limit of a δ-function potential with strength going to infinity [12].

Figure 2 compares computed values of the effective rotational constant (B_{eff}) with experimental results [4,26]. As in the experiments, B_{eff} is defined to be half of the energy difference between the ground state and the lowest excited a-type state [4,19]. The fixed-node diffusion Monte Carlo (FN-DMC) results were obtained using the genetic algorithm DMC method [19]. Results are shown

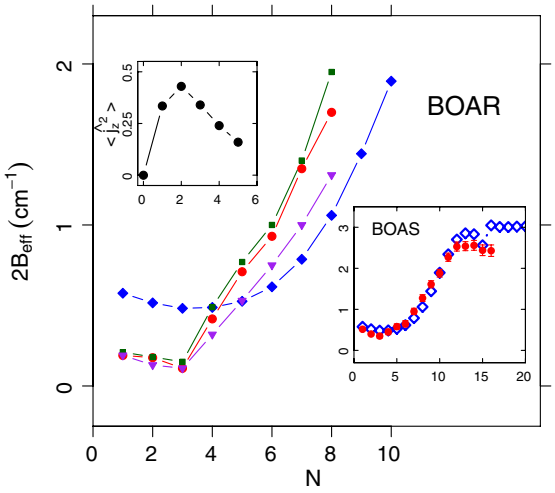

FIG. 2 (color online). Energy splittings ($2B_{eff}$) for a-type, $J = 1 - 0$ rotational transitions as a function of the number of ^{4}He atoms (N). The experimental results are shown as blue diamonds —mm/microwave results [4] for $N \leq 10$ and IR results otherwise [26]. The main panel shows FN-DMC results using the AMcW PES (green squares) and two different forms for the Gaussian barrier with $g_0 = 100$ cm^{-1}, $\alpha = 40$ rad^{-2} (soft barrier, red circles) and $g_0 = 500$ cm^{-1}, $\alpha = 750$ rad^{-2} (hard barrier, purple triangles). For clarity, error bars for the DMC results have been omitted but are provided in the table in the Supplemental Material [25]. The lower inset compares experimental to FN-DMC results in the BOAS model obtained using the soft Gaussian. The AMcW PES leads to almost indistinguishable results in the BOAS case. The upper inset shows $\langle \hat{j}_z^2 \rangle$ as a function of N from the BOAR basis set calculations using the soft Gaussian interaction.

using the AMcW PES and both the hard and soft Gaussian barriers in the BOAR model. Not shown are the accurate results (for $N \leq 5$) obtained using a finite basis set consisting of Bose symmetrized products of eigenfunctions of the operators $\hat{j}_z$ (i.e., $e^{im_j\theta}$) and $\hat{\ell}_{iz}$ (i.e., $e^{im_i\phi_i}$). See the Supplemental Material [25] for tabulated results up to $N = 10$.

To illustrate how well the Gaussian barrier captures the physics, the lower inset in Fig. 2 also compares experimental to FN-DMC results in a "bosons-on-a-sphere" (BOAS) model. In this approximation, the ^{4}He atoms move on the surface of a sphere, and the CO molecule is allowed to rotate in three dimensions. The BOAS Hamiltonian is closer to the full problem than is the BOAR model, and the agreement with experiment is correspondingly better, especially for $N < 10$. The BOAS model is better because it is less simplified and more faithfully reproduces how the ^{4}He density is distributed in three dimensions. However, both the BOAR and BOAS models capture the initial decrease in $B_{\rm eff}$ with an early turnaround at $N \sim 3$–4. The value of N at which the turnaround occurs can be varied by altering the strength or symmetry of the atom-molecule interaction or by varying B_0 artificially. All of the calculations in Fig. 2 are quite congruent with the experimental results. A practical advantage of the BOAR (as compared to the BOAS) model is that accurate basis set calculations are possible for N values that bracket the turnaround in $B_{\rm eff}$. The results of the basis set results up to $N = 5$, reported in the Supplemental Material [25], agree well with the DMC results.

Also shown in Fig. 2 is $\langle \hat{j}_z^2 \rangle$ for the ground state of the BOAR Hamiltonian as a function of N using the soft Gaussian barrier in the basis set calculations. After an early rise to a maximum at $N = 2$, $\langle \hat{j}_z^2 \rangle$ falls quite rapidly with increasing N. Absent any atom-molecule coupling (e.g., $N = 0$), or for an isotropic interaction, $\langle \hat{j}_z^2 \rangle = 0$. Deviations of $\langle j_z^2 \rangle$ from zero (in the ground state) are, therefore, an indicator of the extent of molecule-solvent coupling; i.e., $\hat{j}_z$ is no longer a constant of the motion when anisotropic coupling exists. The decrease in $\langle \hat{j}_z^2 \rangle$ with N therefore demonstrates dynamical decoupling of the molecule. The decoupling is primarily due to the repulsive solvent-solvent interactions because it occurs even when the AMcW He-He potential, which contains both repulsive and attractive branches, is replaced by a purely repulsive Gaussian barrier.

The dynamical decoupling of the solvent suggests that the system might reasonably be modeled as a one-dimensional TG gas confined to a ring and stirred by the molecule; that is, we take the δ-function limit of the Gaussian barrier and drop the term in $\hat{j}_z^2$ in Eq. (1) altogether. It is important to note that the latter step is not an adiabatic approximation based on the different time scales of the solvent and the bare CO molecule. Rather, it is motivated by the basis set calculations, which demonstrate that the molecule decouples substantially even for relatively small values of N. The main reason for making this approximation is that it allows the TDSE to be solved numerically for N particles, thereby allowing the particle current to be computed. The resulting Hamiltonian is

$$\hat{H}_{\rm TG} = -\hbar\omega_0 \sum_{i=1}^{N} \frac{\partial^2}{\partial\phi_i^2} + \sum_{i<k}^{N} g\delta(\phi_i - \phi_k) + \sum_{i=1}^{N} V(\phi_i - \omega_{\rm eff} t). \quad (2)$$

Because the rotational kinetic energy operator for the molecule has been neglected, θ may be replaced semiclassically by $\omega_{\rm eff} t$ where $\omega_{\rm eff}$ is the (variable) angular frequency introduced earlier and t is time. This approximation has the justification that if the rotationally excited molecule is undergoing effective free rotation then the ^{4}He atoms will be subject to a time periodic perturbation. The presence of the δ-function potential allows, in the TG gas limit when $g \to \infty$, the Bose-Fermi (BF) mapping [15,16] to be applied. The relative insensitivity of the results to the hardness of the Gaussian barrier is the reason that the system can be modeled as a TG gas with no need to consider the more complicated (to implement) Lieb-Liniger case [12]. For the ground state, the bosonic wave function is given by

$$\Psi_B(\phi_1, \phi_2, \ldots, \phi_N, t) = \frac{1}{\sqrt{N!}} |\det[\psi_\ell(\phi_i, t)]|, \quad (3)$$

where $\ell, i = 1 \ldots N$. The determinant is a Slater determinant constructed using N orbitals, $\ell = 0 \ldots N-1$ [16], defined as solutions of the TDSE

$$i\hbar \frac{d\psi_\ell(\phi, t)}{dt} = \left(-\hbar\omega_0 \frac{d^2}{d\phi^2} + V(\phi - \omega_{\rm eff} t) \right) \psi_\ell(\phi, t). \quad (4)$$

To compute the current density, the TDSE is integrated numerically with the initial ($t = 0$) states being the N orbitals obtained by solving a form of the Whittaker-Hill equation [27]

$$\left(-\hbar\omega_0 \frac{d^2}{d\phi^2} + a\cos\phi + b\cos 2\phi \right) \psi_\ell(\phi) = E_\ell \psi_\ell(\phi), \quad (5)$$

where $a = V_1(R_0)$, $b = 3V_2(R_0)/4$ and an inessential additive constant have been omitted. The orbitals may be solved for numerically using recurrence relations [27,28]. To demonstrate that the TG limit of the BOAR model is, in fact, a reasonable approximation, we compare directly the BF-mapped Whittaker-Hill wave functions (at $t = 0$) and the accurate BOAR wave functions obtained from the basis set calculations, with $\theta = \omega_{\rm eff} t = 0$. Figure 3 presents sections through the BOAR (using the soft

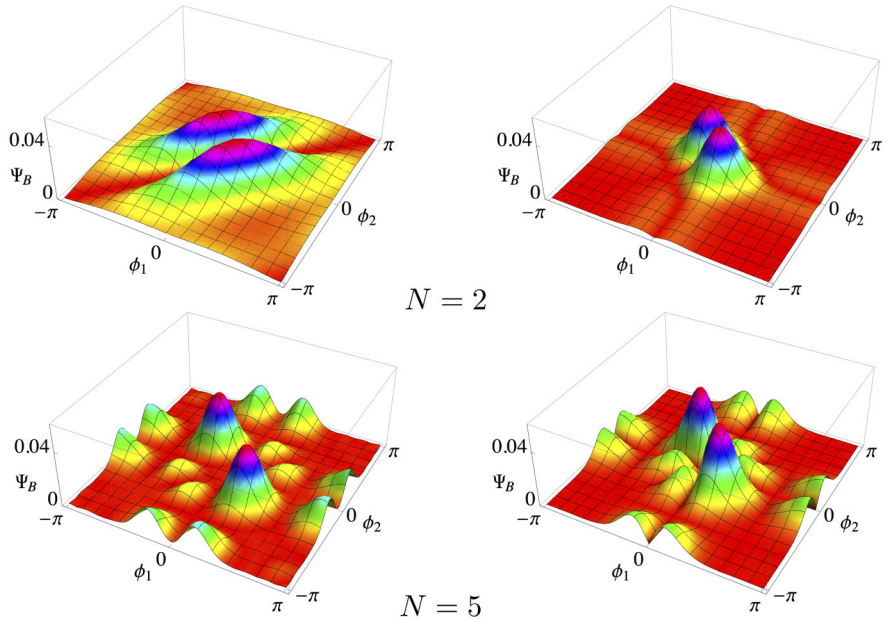

FIG. 3 (color online). Comparison of the ground state bosonic wave functions (Ψ_B) obtained (left) from the basis set calculations for Eq. (1) (using the soft Gaussian barrier) with (right) the BF mapped wave functions [corresponding to Eq. (5)] for $N = 2$ (top) and $N = 5$ (bottom). In the wave functions from the basis set calculations, $\theta = 0$. For $N = 5$, three of the five helium atom angles were fixed. The similarity of the $N = 5$ wave functions is indicative of decoupling of the molecule from the solvent because the BF wave function, unlike the basis set wave function, assumes *a priori* that the molecule has decoupled.

Gaussian barrier) and BF wave functions for $N = 2$ and $N = 5$. For $N = 2$, the BOAR wave function is significantly more delocalized than the BF wave function. At $N = 5$ the agreement is much better, although clearly not perfect. These plots are evidence for the rapid decoupling of the molecule from its environment with increasing N. They also justify taking the TG limit.

The TDSE in Eq. (4) corresponds to a TG gas confined to a ring and stirred by a freely rotating molecule. Similar to Schenke *et al.* [18], who used a δ barrier to stir a TG gas confined to a ring, we calculate the time- and space-averaged current density, F, for a nonadiabatic initial excitation of the molecule at $t = 0$. The TDSE was integrated numerically (after scaling) using as initial states the orbitals obtained by solving Eq. (5) for the $\ell = 0 \ldots 6$ orbitals corresponding to $N = 7$. The TDSE was integrated using a method similar to that described in Ref. [29]. Results were checked using a fast Fourier transform, split-operator procedure [30,31]. We also computed the Floquet quasienergies using generalized Floquet theory [32], and they, together with F, are shown in Fig. 4 as a function of the angular frequency ratio $\omega_{\text{eff}}/\omega_0$.

At integer values of the ratio $\omega_{\text{eff}}/\omega_0$ the Floquet states, starting at $N \sim 4$, show avoided crossings similar to those discovered in Ref. [18]. These states become coupled by the molecule that opens up gaps at integer values of $\omega_{\text{eff}}/\omega_0$. This allows for the population of higher AM states and thereby current excitation. The structure of the Floquet spectrum thus accounts for the peaks in the integrated current density also shown in Fig. 4. It is significant that the avoided crossings first appear when the molecule has significantly decoupled from its environment, i.e., close to the onset of microscopic superfluidity. Away from integer values of $\omega_{\text{eff}}/\omega_0$, the flux

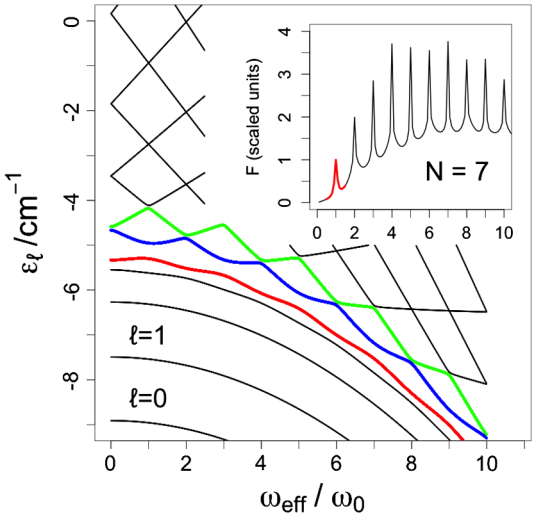

FIG. 4 (color online). Floquet eigenvalues ϵ_ℓ (where ℓ labels the Floquet mode [32]) as a function of the ratio $\omega_{\text{eff}}/\omega_0$. Orbital energies corresponding to $\ell = 4, 5, 6$ are shown bolded (online: red, blue, and green, respectively). The inset shows the long-time flux average, F, obtained by propagating the time-dependent BF wave function for $N = 7$. The flux averaging was done as described in the text and in Ref. [18]. The threshold peak for stirring, normalized to unity, is bolded (red online).

plot indicates that the TG gas is harder to stir. There also exists a velocity threshold for current generation at $\omega_{\mathrm{eff}}/\omega_0 = 1$, which is indicative of superfluid behavior. However, unlike in Ref. [18], below this threshold, F is not exactly zero, nor is it zero between subsequent peaks. Rather, the background current increases and eventually saturates. This predicts that B_{eff} will converge to a nanodroplet limiting value lower than B_0, which is consonant with both experiment and previous quantum Monte Carlo studies [19–21]. That is, the molecular impurity will experience a drag force even at 0 K. Similar behavior at 0 K has been noted previously in a quasi-1D Bose-Einstein condensate [13].

In summary, the BOAR model shows that the decoupling of the molecule can be traced primarily to the interplay between the purely repulsive interactions between the bosonic ^{4}He atoms and the strength and symmetry of the molecule-solvent interaction. Solving the TDSE in the TG limit reveals a drag force at 0 K together with a threshold for stirring. Because the energy spectra for 1D hard-core bosons and fermions are identical [15], any significant differences between purely repulsive-doped 1D fermionic ^{3}He and bosonic ^{4}He atoms confined to a ring must arise because of differences in the decoupling mechanism (that is, if decoupling occurs at all for ^{3}He [1,5,6,33]). For fermions (^{3}He) the attractive part of the He-He PES may play a role by providing a pairing mechanism [34].

This work was supported, in part, by Grant No. CHE1300504 from the National Science Foundation to D. F. at Utah State University. We thank a referee for pointing out an article that finds the exact ground state for a Bose-Einstein condensate on a ring [35].

*Corresponding author.
david.farrelly@usu.edu

[1] S. Grebenev, J. P. Toennies, and A. F. Vilesov, Science **279**, 2083 (1998).
[2] E. Lee, D. Farrelly, and K. B. Whaley, Phys. Rev. Lett. **83**, 3812 (1999).
[3] C. Callegari, K. K. Lehmann, R. Schmied, and G. Scoles, J. Chem. Phys. **115**, 10090 (2001).
[4] L. A. Surin, A. V. Potapov, B. S. Dumesh, S. Schlemmer, Y. Xu, P. L. Raston, and W. Jäger, Phys. Rev. Lett. **101**, 233401 (2008).
[5] L. A. Surin, JETP Lett. **97**, 57 (2013).
[6] J. P. Toennies, Mol. Phys. **111**, 1879 (2013).
[7] P. L. Raston, Y. Xu, W. Jäger, A. V. Potapov, L. A. Surin, B. S. Dumesh, and S. Schlemmer, Phys. Chem. Chem. Phys. **12**, 8260 (2010).
[8] H. Li, R. J. LeRoy, P.-N. Roy, and A. R. W. McKellar, Phys. Rev. Lett. **105**, 133401 (2010).
[9] C. Callegari, W. Jäger, and F. Stienkemeier, in *Handbook of Nanophysics: Nanoparticles and Quantum Dots*, edited by K. D. Sattler (CRC Press, Taylor and Francis Group, Boca Raton, FL, 2011), Chap. 4, p. 4.1.
[10] P. L. Raston, W. Jäger, H. Li, R. J. Le Roy, and P.-N. Roy, Phys. Rev. Lett. **108**, 253402 (2012).
[11] S. P. Dempster, O. Sukhorukov, Q.-Y. Lei, and W. Jäger, J. Chem. Phys. **137**, 174303 (2012).
[12] A. Yu. Cherny, J.-S. Caux, and J. Brand, Front. Phys. **7**, 54 (2012).
[13] A. G. Sykes, M. J. Davis, and D. C. Roberts, Phys. Rev. Lett. **103**, 085302 (2009).
[14] M. D. Girardeau and G. E. Astrakharchik, Phys. Rev. Lett. **109**, 235305 (2012).
[15] M. Girardeau, J. Math. Phys. (N.Y.) **1**, 516 (1960).
[16] M. D. Girardeau, E. M. Wright, and J. M. Triscari, Phys. Rev. A **63**, 033601 (2001).
[17] T. Kinoshita, T. Wenger, and D. S. Weiss, Science **305**, 1125 (2004).
[18] C. Schenke, A. Minguzzi, and F. W. J. Hekking, Phys. Rev. A **85**, 053627 (2012).
[19] J. A. Ramilowski and D. Farrelly, Phys. Chem. Chem. Phys. **14**, 8123 (2012).
[20] A. A. Mikosz, J. A. Ramilowski, and D. Farrelly, J. Chem. Phys. **125**, 014312 (2006).
[21] P. Cazzato, S. Paolini, S. Moroni, and S. Baroni, J. Chem. Phys. **120**, 9071 (2004).
[22] K. K. Lehmann, J. Chem. Phys. **114**, 4643 (2001).
[23] C. E. Chuaqui, R. J. LeRoy, and A. R. W. McKellar, J. Chem. Phys. **101**, 39 (1994).
[24] R. A. Aziz, F. R. W. McCourt, and C. C. K. Wong, Mol. Phys. **61**, 1487 (1987).
[25] See Supplemental Material at http://link.aps.org/supplemental/10.1103/PhysRevLett.112.143401 for a table containing the basis set results and the data used to construct Fig. 2.
[26] J. Tang and A. R. W. McKellar, J. Chem. Phys. **119**, 754 (2003).
[27] L. F. Roncaratti and V. Aquilanti, Int. J. Quantum Chem. **110**, 716 (2010).
[28] S. M. Parker, M. A. Ratner, and T. Seideman, J. Chem. Phys. **135**, 224301 (2011).
[29] J. C. Ross and H. W. Capel, Physica (Amsterdam) **287A**, 217 (2000).
[30] D. Kosloff and R. Kosloff, J. Comput. Phys. **52**, 35 (1983).
[31] R. Chacón, F. Borondo, and D. Farrelly, Europhys. Lett. **86**, 30004 (2009).
[32] M. Grifoni and P. Hänggi, Phys. Rep. **304**, 229 (1998).
[33] B. G. Sartakov, J. P. Toennies, and A. F. Vilesov, J. Chem. Phys. **136**, 134316 (2012).
[34] M. D. Girardeau and A. Minguzzi, Phys. Rev. Lett. **96**, 080404 (2006).
[35] K. Sakmann, A. I. Streltsov, O. E. Alon, and L. S. Cederbaum, Phys. Rev. A **72**, 033613 (2005).